Neutron imaging of froth structure and particle motion

Heitkam, S.; Rudolph, M.; Lappan, T.; Sarma, M.; Eckert, S.; Trtik, P.; Lehmann, E.; Vontobel, P.; Eckert, K.;

Originally published:

April 2018

Minerals Engineering 119(2018), 126-129

DOI: https://doi.org/10.1016/j.mineng.2018.01.021

Perma-Link to Publication Repository of HZDR:

https://www.hzdr.de/publications/Publ-26164

Neutron imaging of froth structure and particle motion

Sascha Heitkam[a,b,*], Martin Rudolph[c], Tobias Lappan[b], Martins Sarma[b], Sven Eckert[b], Pavel Trtik[d], Eberhard Lehmann[d], Peter Vontobel[d], Kerstin Eckert[a,b]

[a] *Technische Universität Dresden, Institute of Process Engineering and Environmental Technology, 01062 Dresden, Germany*
[b] *Helmholtz-Zentrum Dresden-Rossendorf, Institute of Fluid Dynamics, 01328 Dresden, Germany*
[c] *Helmholtz Institute Freiberg for Resource Technology, 09599 Freiberg, Germany*
[d] *Paul Scherrer Institut, 5232 Villigen PSI, Switzerland*

Abstract

This article reports on the simultaneous measurement of foam structure and attached particles employing neutron imaging. An aqueous foam sample is placed in the NEUTRA beamline at PSI, enabling a spatial resolution of less than 200 μm to be achieved at a frame rate of more than 1 Hz. A forced drainage setup allows the liquid content of the foam to be controlled. The averaged attenuation of the neutrons is demonstrated to yield the liquid fraction of the foam. Hydrophobized gadolinium particles with a diameter of 200 μm are added to the foam. Using two surfactants, different levels of hydrophobicity are achieved. Depending on the drainage flow and the hydrophobicity, the particles are washed out of the foam at different rates. An avalanche-like motion of particle clusters is observed. Neutron radiography is demonstrated to yield unique insights into the unsteady froth flotation process.

Keywords: Neutron imaging, Flotation, Froth, Particle Tracking

1. Introduction

Froth flotation, exploiting differences in surface properties of mineral particles, is the most important process in ore beneficiation in mineral processing. In the froth zone, the bubble-particle aggregates, crossing the pulp-froth interface, move upwards towards the concentrate launder [1, 2]. Additionally, hydrophilic particles are non-selectively entrained into the froth, driven by the turbulence in the pulp. Counterflowing wash water sprayed on top of the froth is able to reduce the transport of these undesired fractions into the concentrate. It is obvious that improving the recovery and the grade of the flotation concentrate requires a refined understanding of the froth dynamics, including drainage, the bursting and coalescence of bubbles and the respective impact on particle motion. This also requires the availibility of reliable experimental data. However, local measurements and detection of particles in flotation froths are challenging due to their opaqueness. Phosphorescent tracer particles were applied to determine the dispersion of hydrophilic particles in the froth in [3]. Particle tracking velocimetry was used in [4] to analyse particle sedimentation in dependence on the foam structure. The rheology of froth, coupled to optical inspection, was studied in [5]. However, the applications of these optical techniques is limited to transparent foams of low thickness. To overcome these restrictions, positron emission particle tracking has been established as an attractive technique to analyse particle paths in the froth [6, 7]. However, high-speed imaging of the froth is mandatory to be able to correlate particle trajectories with the foam and froth structure. By applying neutron imaging, we introduce a promising technique for froth studies which overcomes the limitations of all previously mentioned techniques. Neutron imaging is capable of tracking the motion of selected particles, both hydrophilic and hydrophobic, and of characterizing the local foam structure. Compared to optical measurement techniques, neutron imaging allows the investigation of thicker froth samples and higher liquid fractions, because the neutrons are not refracted by the gas-liquid interfaces. The main advantage over X-ray imaging is, that water has a roughly 30 times higher attenuation coefficient for neutrons (25 meV) than for X-rays (150 keV) [8, 9], yielding high-contrast images of the thin foam structure at reasonable frame rates.

2. Experimental Setup

2.1. Measuring configuration

Measurements were carried out at the Paul Scherrer Institut in Villigen, Switzerland. The NEUTRA beam line of the neutron spallation source SINQ was employed [10], providing approximately $1.0 \times 10^7\,\mathrm{cm^{-2}s^{-1}}$ of thermal neutron flux at 25 meV. The distance between measurement position 2 and the beam defining aperture (Ø20 mm) equals 7000 mm. Similarly to X-rays, the neutrons penetrate matter and are attenuated at

*Corresponding author
Email address: sascha.heitkam@tu-dresden.de (Sascha Heitkam)

the contained elements. In contrast to X-rays, neutrons are attenuated at the atomic nucleus rather than at the electrons. Therefore, the attenuation coefficient does not increase in line with the atomic number, but is also high for some light atoms, e.g. hydrogen and boron. The measurement object is placed inside the neutron beam. The unattenuated neutrons hit a scintillator screen of $14 \times 14\,\mathrm{cm}^2$ area, generating visible light. This light is captured by means of a sCMOS camera with 2048×2048 px @ 5 fps, yielding a radiographic image of the measurement object. More details on the beam line are given in [11].

The measurement object is a glass cuvette with a triangular cross section, partially filled with liquid. Blowing air through four nozzles at the bottom, bubbles of a diameter $D_b = (5 \pm 1)\,\mathrm{mm}$ are injected, filling the cuvette with foam. Using three needles positioned at the top, a steady flow of liquid is applied, draining downward through the foam. Wetted gadolinium (Gd) particles (Section 2.2) are introduced via an additional tube between the needles. After each run, visual checks are carried out to ensure that no particle clusters are stuck at the glass wall.

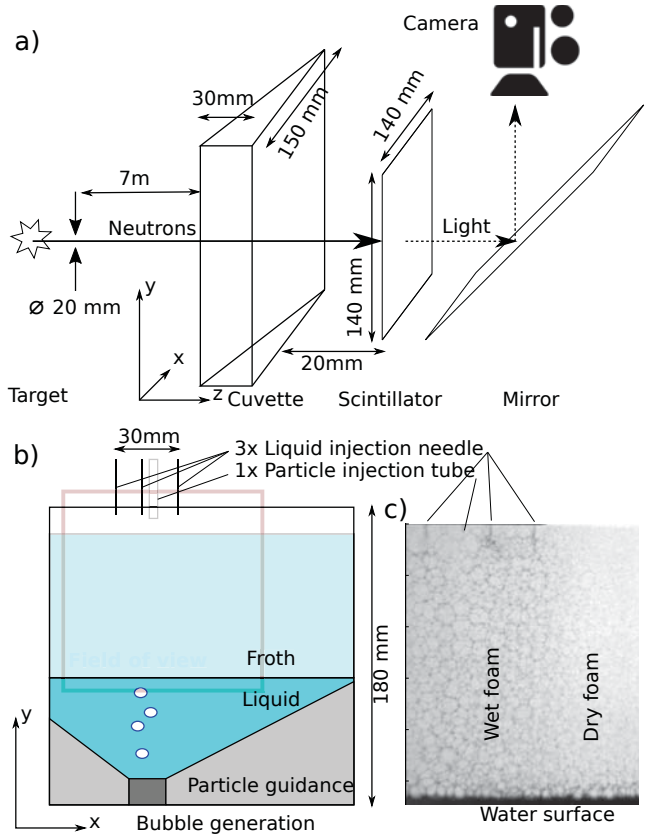

Figure 1: Setup of neutron imaging (a), foaming inside the cuvette (b) and foam image (c).

2.2. Particle selection and image contrast

The measurements are carried out using a dispersion of hydrophobic, irregularly shaped Gd particles (Section 2.3) in aqueous liquid. The Gd particles are assumed to exhibit a thin oxidized surface (Gd_2O_3) with negligible influence on the neutron attenuation. Gd has the largest neutron attenuation coefficient ($\sigma_{Gd} = 1479.04\,\mathrm{cm}^{-1}$) of all the elements [9]. Even small Gd particles of 200 μm diameter attenuate all but 1×10^{-11} % of the neutrons. Figure 2 shows a sample image of a large cluster of such particles. More details on the particle selection criteria are given in the supplemental materials [12]. The attenuation coefficient of pure water equals $\sigma_{H2O} = 3.74\,\mathrm{cm}^{-1}$. The dissolved surfactants have a negligible influence of less than 1 % on this value. A water structure with a thickness of 1 mm attenuates approximately 31 % of the beam intensity. However, the low neutron rate per pixel causes a low signal-to-noise ratio (SNR). A wiener2 noise reduction [13] and subsequent Gaussian filtering in time ($\sigma_t = 200\,\mathrm{ms}$) are applied to visualize the foam structure. Figure 2 demonstrates the filtering effect on a particle cluster attached at a fixed position at the container wall and on dry and wet foam (middle and bottom rows) The foam has a thickness of 25 mm and about $\Phi = 0.6\%$ and $\Phi = 1.6\%$ liquid content, respectively.

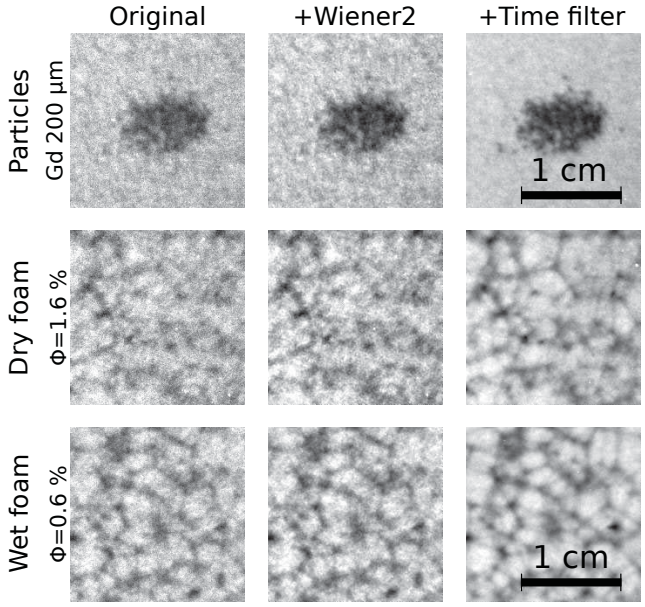

Figure 2: Image processing by means of Wiener2 noise reduction and subsequent time filtering. Effect on cluster of particles, dry foam and wet foam is shown.

2.3. Particle treatment

To mimic a flotation process, the Gd particles are hydrophobised. To that end, 2.5 g particles are added to 100 ml of deionized water with 0.01 mol/L KCl and 0.002 mol/L Sodium Oleate (NaOl), and stirred for 15 minutes. The level of hydrophobicity is evaluated in a prestudy by submerging a 0.25 μl air bubble for 1 second in the sediment bed, then pulling it out and taking a picture of the attached particles (Figure 3). Treated particles show much greater hydrophobicity (Figure 3b) than

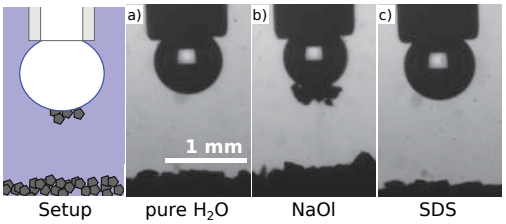

Figure 3: Hydrophobicity of Gd particles in pure water (a), treated with KCl + NaOl (b) and treated with KCl + NaOl in SDS (c).

untreated particles in pure water (Figure 3a). However, adding 0.0087 mol/L sodium dodecyl sulfate (SDS) again reduces the hydrophobicity (Figure 3c), rendering the particles hydrophilic again.

3. Results

In the first step, the attenuation of aqueous SDS foam with large bubbles under a steady drainage flow without particles is investigated. This measurement validates the capability of neutron imaging to measure the distribution of liquid content inside the foam or froth. Sample images are shown in Figure 2. The measured intensity is averaged in time and over a $2 \times 2\,\mathrm{cm}^2$ section below the drainage injection point. The average intensity is compared with a reference for the empty cuvette, yielding the relative attenuation of the foam for different drainage flow rates Q per horizontal area S. The values are given in Figure 4. The estimation in Figure 4 is based on Darcy's law [15]

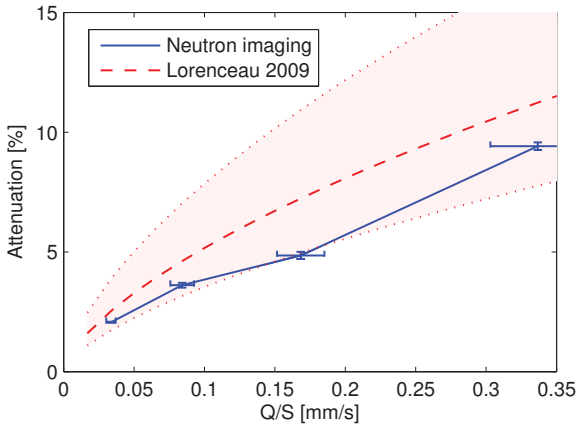

Figure 4: Attenuation of aqueous foam for different drainage flow measured with neutron imaging and compared to estimated attenuation from literatur values on foam drainage [14]. The shaded area marks the scatter througout literature.

and the drainage resistance k of SDS foam with certain liquid contents Φ [16, 14]

$$k = 6.7 \times 10^{-4} \Phi^{3/2} D_b^2. \quad (1)$$

Subsequently, the attenuation is estimated assuming that the liquid is homogeneously distributed in the test section and applying the Beer-Lambert law [17]. Uncertainties mainly result from the large scatter of drainage literature values [14] and the unknown cross-sectional area of the drainage flow. In general, our measured values are situated within the typical range of literature values. Also, the stricly increasing attenuation is reproduced. This allows the distribution of liquid in a foam sample to be evaluated. The systematically higher values for the estimated attenuation could result from the assumption of homogeneously distributed liquid content $\overline{\Phi}$ inside the Beer-Lambert law ($1 - e^{-\overline{\Phi}} \geq \overline{1 - e^{-\Phi}}$). In the next step, particle-laden foam is considered. As mentioned above, the Gd particles are treated with NaOl to ensure their hydrophobicity. Moreover, two different foaming agents (NaOl, SDS) are employed in the cuvette, yielding different levels of hydrophobicity. In all cases, approximately $10\,\mu$L of the suspension of conditioned Gd particles are added to the foam after drainage and measurement is started. Applying threshold binarisation and segmentation, particle clusters are detected. The downward movement of the center of mass of the particle cluster is evaluated over time. Figure 5 shows the downward velocity for both foaming agents and different drainage velocities. In the less hydrophobic case

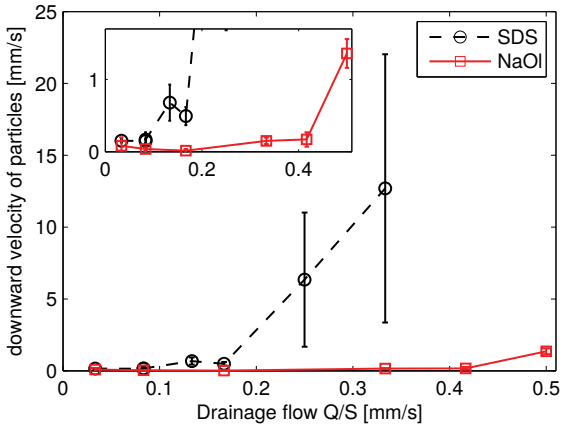

Figure 5: Downward velocity of the center of mass of the particle clusters, situated inside the froth, as a function of the steady drainage flow used for both surfactants. The inset shows a magnified image of the small values.

of SDS foam, the particles are flushed out of the foam at much lower drainage flow rates ($Q \approx 0.17\,\mathrm{m/s}$) than with NaOl foam ($Q \approx 0.4\,\mathrm{m/s}$). However, the absolute numbers suffer from large uncertainties. At a higher drainage, clusters are removed from the foam into the pulp, not contributing to the center of mass any longer. Also, at higher liquid content the foam starts to move due to the convective instability [18]. And finally, the clusters do not move continuously through the foam but in avalanches, yielding high statistical uncertainties. However, these uncertainties do not endanger the proof of principle. They can be reduced by averaging on a steady-state experiment and avoiding froth movement.

Figure 6 shows the movement of one cluster at

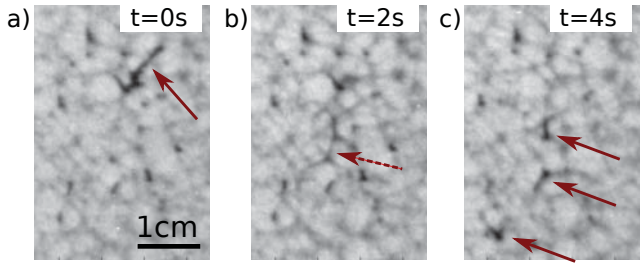

Figure 6: Avalanche-like movement of particle clusters. Clusters rest in foam vertices (a), and are eventually flushed downward, potentially splitting at vertices (b) and forming one or more resting clusters again (c).

8 ml/min drainage flow in SDS foam. The particle clusters are situated in the vertices of the foam structure (Figure 6a). Eventually, they are fluidized and flushed downward along the Plateau borders (Figure 6b). At vertices, the avalanche sometimes splits into two or more streams. At medium drainage flow rates, the avalanche stops after passing one or several Plateau borders and the particles reform a cluster in a vertex (Figure 6c).

4. Discussion

The neutron imaging technique is applicable to carry out a quantitative investigation into the interaction of drainage flow with attached particles in froth. Therefore, neutron imaging is able to give valuable insights into froth flotation. Including the applied filtering, frame rates above 1 Hz and spatial resolutions below 200 μm were achieved. The average distribution of water is clearly visible, and can be analyzed quantitatively. This visualization of foam structures allows conclusions to be drawn about the positioning and the movement of particles inside the foam. Steady or slowly moving Gd particles and particle clusters can be tracked reliably. In the present configuration level of neutron imaging at the NEUTRA beamline, it was not possible to count the exact number of particles within one cluster, biasing quantitative analysis. Also, when a cluster flushes quickly through a Plateau border, the current frame rate is too low to track this movement. Approaches for the increase of the available neutron flux that would allow dynamic neutron imaging with higher frame rates to be used and/or an improved signal-to-noise ratio are foreseen for future investigations [19]. We can thus expect the surveying of foam structures and particle clusters at even higher precision.

Acknowledgements

The support of the DECHEMA (MBFSt-3534) and of the German Research Foundation (HE 7529/1-1) is gratefully acknowledged. The authors would like to thank the Neutron Imaging & Activation Group, PSI, Switzerland, for the valuable help for operating neutron radiography. We also thank our colleagues from NetFlot (KIC RawMaterials project no. 15062, infrastructure network "Modelling of flotation processes") for valuable discussions.

References

[1] A. Nguyen, H. J. Schulze, Colloidal science of flotation, Vol. 118, CRC Press, 2003.
[2] S. Ata, Phenomena in the froth phase of flotation — A review, International Journal of Mineral Processing 102-103 (2012) 1–12.
[3] S. Ata, S. Pigram, G. Jameson, Tracking of particles in the froth phase: An experimental technique, Minerals engineering 19 (6) (2006) 824–830.
[4] N. Bennani, A. Fujiwara, S. Takagi, Y. Matsumoto, Coarse particles sedimentation within a quasi two-dimensional rising foam, Colloids and Surfaces A: Physicochemical and Engineering Aspects 309 (1) (2007) 7–12.
[5] C. Li, K. Runge, F. Shi, S. Farrokhpay, Effect of flotation froth properties on froth rheology, Powder Technology 294 (2016) 55–65.
[6] K. Waters, N. Rowson, X. Fan, D. Parker, J. Cilliers, Positron emission particle tracking as a method to map the movement of particles in the pulp and froth phases, Minerals Engineering 21 (12) (2008) 877–882.
[7] K. Cole, K. Waters, X. Fan, S. Neethling, J. Cilliers, Combining positron emission particle tracking and image analysis to interpret particle motion in froths, Minerals Engineering 23 (11) (2010) 1036–1044.
[8] J. H. Hubbell, S. M. Seltzer, Tables of x-ray mass attenuation coefficients and mass energy-absorption coefficients 1 kev to 20 mev for elements z= 1 to 92 and 48 additional substances of dosimetric interest, Tech. rep., National Inst. of Standards and Technology-PL, Gaithersburg, MD (United States). Ionizing Radiation Div. (1995).
[9] V. F. Sears, Neutron scattering lengths and cross sections, Neutron news 3 (3) (1992) 26–37.
[10] P. S. Institut, Neutron imaging at the spallation source sinq (2016).
[11] L. W. E. H. Lehmann, P. Vontobel, Properties of the radiography facility neutra at SINQ and its potential for use as european reference facility, Tech. rep., Paul Scherrer Institut (2007).
[12] S. Heitkam, Guideline for particle chioice, Supplemental Materials.
[13] J. S. Lim, Two-dimensional signal and image processing, Englewood Cliffs, NJ, Prentice Hall, 1990, 710 p. (1990) p. 548.
[14] E. Lorenceau, N. Louvet, F. Rouyer, O. Pitois, Permeability of aqueous foams, The European Physical Journal E: Soft Matter and Biological Physics 28 (3) (2009) 293–304.
[15] S. Whitaker, Flow in porous media I: A theoretical derivation of Darcy's law, Transport in porous media 1 (1) (1986) 3–25.
[16] A. Saint-Jalmes, Y. Zhang, D. Langevin, Quantitative description of foam drainage: Transitions with surface mobility, The European Physical Journal E: Soft Matter and Biological Physics 15 (1) (2004) 53–60.
[17] K. Fuwa, B. Valle, The physical basis of analytical atomic absorption spectrometry. The pertinence of the Beer-Lambert law., Analytical Chemistry 35 (8) (1963) 942–946.
[18] S. Hutzler, D. Weaire, R. Crawford, Convective instability in foam drainage, EPL (Europhysics Letters) 41 (4) (1998) 461.
[19] P. Trtik, M. Morgano, R. Bentz, E. Lehmann, 100Hz neutron radiography at the BOA beamline using a parabolic focussing guide, MethodsX 3 (2016) 535–541.